SEISMIC DESIGN SPECTRA FOR FRICTION-DAMPED STRUCTURES

By A. Filiatrault,[1] Associate Member, ASCE, and S. Cherry,[2] Fellow, ASCE

ABSTRACT: A simplified seismic design procedure is proposed for structures equipped with an innovative friction-damping system. The system has been shown experimentally to perform very well and could represent a major new development in earthquake-resistant design. This paper first presents an efficient modeling approach for the seismic analysis and design of friction-damped structures. The hysteretic properties of the friction dampers are derived theoretically and are included in a Friction Damped Braced Frame Analysis Program (FDBFAP), which is adaptable to a microcomputer environment. FDBFAP is then used to perform a parametric study of the optimum slip-load distribution for the friction dampers. The results of the study lead to the construction of a design slip-load spectrum for the rapid evaluation of the optimum slip-load distribution. The spectrum takes into account the properties of the structure and of the ground motion anticipated at the construction site. The availability of this design slip-load spectrum should lead to a greater acceptance by the engineering profession of this innovative design concept.

INTRODUCTION

Recently, a novel structural system for the aseismic design of framed buildings was proposed by Pall and Marsh (1982). The system consists of an inexpensive mechanism containing friction brake lining pads introduced at the intersection of frame cross braces. Fig. 1 shows the location of the friction devices in a typical steel frame and the general arrangement of an actual friction device.

A typical hysteresis loop developed from prototypes of these friction dampers (Filiatrault and Cherry 1987) is shown in Fig. 2. The hysteresis loop is very nearly a perfect rectangle and exhibits negligible fade even after 50 cycles.

During severe seismic excitations, the mechanism slips at a predetermined load, before any yielding of the main members has occurred. Slipping of a damper changes the natural frequency of the structure and allows the structure to dissipate the input seismic energy mechanically, by friction. The friction-damping system has been shown experimentally to perform reliably and to reduce significantly the seismic response of conventional structures (Filiatrault and Cherry 1987).

Some of these dampers are being installed now in a structure in Canada, (Pall et al. 1987). However, the techniques used for design are expensive and tedious and not readily practical for most design offices. It is therefore essential to develop a simplified seismic design method for this new damping system.

The research presented in the present paper is concerned with the development of such a procedure. The objective is to provide practicing engineers

[1]Asst. Prof., Dept. of Civ. Engrg., Univ. of British Columbia, Vancouver, B.C., Canada, V6T 1W5.

[2]Prof., Dept. of Civ. Engrg., Univ. of British Columbia, Vancouver, B.C., Canada.

Note. Discussion open until October 1, 1990. To extend the closing date one month, a written request must be filed with the ASCE Manager of Journals. The manuscript for this paper was submitted for review and possible publication on August 19, 1988. This paper is part of the ***Journal of Structural Engineering***, Vol. 116, No. 5, May, 1990. ©ASCE, ISSN 0733-9445/90/0005-1334/$1.00 + $.15 per page. Paper No. 24665.

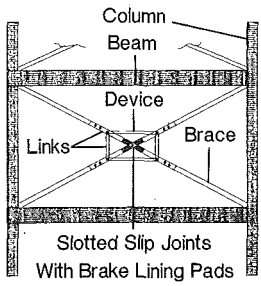

FIG. 1. Typical Location and General Arrangement of Friction Dampers

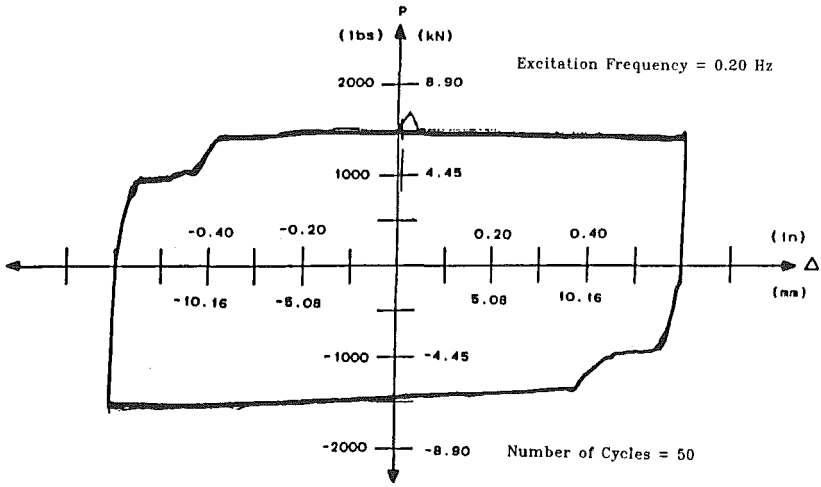

FIG. 2. Typical Measured Hysteresis Curve of Friction Damper

with a simple and direct approach to the seismic design of friction-damped braced frames (FDBF).

Behavior of Friction Dampers

If the diagonal braces of an ordinary braced-frame structure were designed not to buckle in compression, a simple slotted friction joint could be inserted in each diagonal. In such a case, each slip joint would act independently of the other. However, it is frequently not economical to design the braces in compression and, more often, since the braces are quite slender, they are designed to be effective in tension only. In such cases, a simple friction joint would slip in tension but would not slip back during reversal of the tension load or in the compression (buckled) regime. The energy absorption therefore would be relatively poor, since the brace would not slip again until it is stretched beyond its previous elongated length. It is possible to essentially double the energy-absorption capability of the structure through the use of the following friction-damping mechanism.

Consider the hysteretic behavior of a simple FDBF during one cycle of

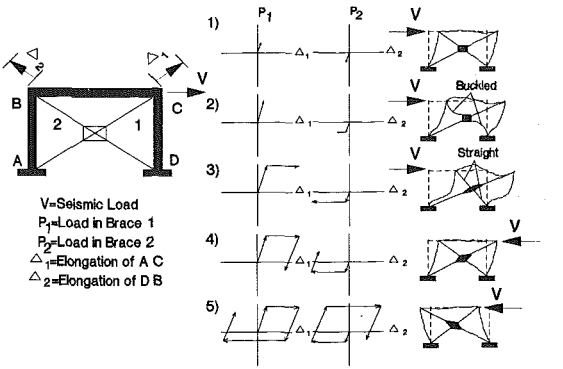

FIG. 3. Hysteretic Behavior of Simple Friction-Damped Braced Frame during One Cycle of Loading

seismic loading as shown in Fig. 3. Let V = lateral load at the girder level representing the seismic load; Δ_1 = relative displacement of node C with respect to node A (defined as positive in Fig. 3); Δ_2 = relative displacement of node B with respect to node D (defined as positive in Fig. 3); P_1 = load in brace 1 (positive in tension); and P_2 = load in brace 2 (positive in tension).

Five stages during a typical load cycle are illustrated in this figure. The load-deformation curves of both braces and the associated deformed shape of the frame are shown for each stage. The following points should be noted during the cycle:

1. In the very early stages of loading, both braces are active and behave elastically in tension and compression.
2. At very low load, the compression brace buckles while the tension brace continues to stretch elastically.
3. The damper is set to slip before yielding occurs in the tension brace. When slippage occurs, the four links of the special mechanism are activated and deform into a rhomboid shape; this deformation pattern is assumed to eliminate the buckled shape of the compression brace. Thus, at the end of the slippage, P_2 is still the buckling load but now the compression brace is straight.
4. When the load is reversed, this straightened brace can immediately absorb energy in tension.
5. After the completion of one cycle the resulting areas of the hysteresis loops for both braces are identical. In this way, the energy dissipated is equal to the energy absorbed in simple friction joints used with braces that are designed not to buckle in compression.

Concept of Optimum Slip-Load Distribution

The total energy dissipated by friction in an FDBF is equal to the product of the slip load and the total slip travel of each friction damper, summed over all the dampers. For very high slip loads, the energy dissipation in friction is zero, as there is no slippage. In this situation, the structure behaves exactly as a conventional braced frame. If the slip loads are small, large slip travels occur but the amount of energy dissipation again is neg-

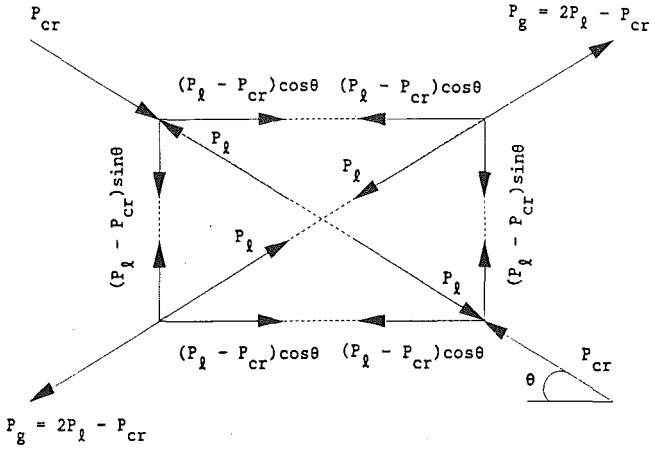

FIG. 4. Free-Body Diagram of Friction Damper when Slippage Occurs

ligible. In this case, the structure behaves exactly as an unbraced frame. Between these extremes, there is an intermediate slip load distribution that results in optimum energy dissipation. This intermediate distribution is defined as the optimum slip-load distribution.

Fig. 4 shows a free-body diagram of a friction damper when slippage occurs. The global slip load (P_g) is defined as the load in the tension brace when slippage occurs, while the local slip load (P_l) is defined as the corresponding load in each friction pad.

As can be seen from equilibrium requirements in Fig. 4, the relation between the global slip load and the local slip load is given by

$$P_g = 2P_l - P_{cr} \quad \ldots\ldots (1)$$

where P_{cr} = critical buckling load of the compression brace.

The design of a building equipped with these friction devices involves the determination of the optimum slip-load distribution to minimize structural response. The optimum slip-load distribution of a friction-damped structure is currently evaluated by a series of time-step dynamic analyses using the well-known general-purpose computer program DRAIN-2D (Kannan and Powell 1973). In this program, the friction devices are modeled as an assemblage of axial and bending elements with pseudo yielding characteristics (Filiatrault and Cherry 1988a). This technique is tedious, requires extensive mainframe computer time and is not readily practical for most design offices. These shortcomings can be avoided by developing a simple alternative computer program, which is adaptable to a microcomputer environment, to perform the required analysis.

Computer Program Description

A specialized computer program that is adaptable to a microcomputer environment was created specifically for the efficient analysis and design of friction-damped braced frames by Filiatrault and Cherry (1989). The hysteretic properties of the friction dampers were derived theoretically and included in this Friction Damped Braced Frame Analysis Program (FDBFAP).

FDBFAP assumes that the beams and columns in a frame remain elastic, and that the inelastic deformations are due only to the slipping of the friction pads and the buckling in compression of the diagonal braces. All possible deformation states of a friction damper are considered, and the resulting global tangent-stiffness matrix of the structure is calculated. The Newmark-Beta method with a constant acceleration algorithm is used to integrate the equations of motion.

The program automatically performs a series of dynamic-response analyses of a FDBF of arbitrary configuration for specified distributions of slip load. For each slip-load distribution, the program calculates the time history of the strain energy in the structure and determines a relative performance index (RPI), which is defined as:

$$\mathrm{RPI} = \frac{1}{2}\left(\frac{\mathrm{SEA}}{\mathrm{SEA}_{(0)}} + \frac{U_{\max}}{U_{\max(0)}}\right) \quad (2)$$

where SEA = strain energy area = area under the strain-energy time history for a friction-damped structure; $\mathrm{SEA}_{(0)}$ = strain energy area for the identical structure, but without bracing (slip load = 0); $U_{\max}$ = maximum strain energy for a friction-damped structure; $U_{\max(0)}$ = maximum strain energy for the identical structure, but without bracing (slip load = 0). The optimum slip load distribution of the structure is defined to be the distribution slip load for which the RPI is a minimum.

Values of the relative performance index (RPI) are such that if RPI = 1, the response corresponds to the behavior of an unbraced structure (slip load = 0); RPI < 1, the response of the friction-damped structure is "smaller" than the response of the unbraced structure; RPI > 1, the response of the friction-damped structure is "larger" than the response of the unbraced structure.

Originally, various parameters (interstory drift, maximum base shear, etc.) were considered in the optimization of the local slip-load distribution. Preliminary analyses showed that the optimum slip load obtained on the basis of these different parameters did not change significantly so that the resulting variation in structural response was observed to be small.

Note that Eq. 2 is based on the elastic strain energy and is not an exact representation of the performance of the structure for small (approaching the unbraced condition) and large (approaching the ordinary braced condition) values of slip load, during which yielding may take place in the beams and columns. However, past investigations (Filiatrault and Cherry 1987, 1988a; Pall and Marsh 1982; Pall et al. 1987) have shown that a FDBF tuned to its optimum slip-load distribution remains elastic and free from permanent damage when excited by severe ground motions. Therefore, to save computing time, hysteretic energy dissipation has not been included in FDBFAP, since only the optimum slip-load response is of interest.

Numerical Example

A representative regular low-rise steel industrial building is to be retrofitted with the new friction damping system. The original building was designed according to earlier code requirements (Montgomery and Hall 1979); the structural layout is shown in Fig. 5. The results of FDBFAP are compared with those obtained from DRAIN-2D.

In the DRAIN-2D analyses, two structural models are considered. The first one is an "exact" model of the example structure; it assumes 3 degrees

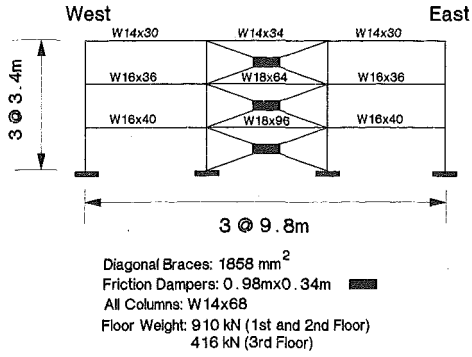

FIG. 5. Low-Rise Steel Industrial Building

of freedom per node, nonlinear beam-column elements with axial load-moment interaction surfaces, and second-order load-sway effects. The second model analyzed by this program incorporates the same assumptions used in FDBFAP: (1) The total mass of the structure is concentrated at the floors, with vertical and rotational inertia neglected; (2) the axial deformations of the beams and columns are neglected; (3) the main structural elements (beams and columns) of the structure remain elastic at all times. For this second case, the dynamic response results obtained using the DRAIN-2D program should be identical to the ones obtained from FDBFAP.

The Newmark-Blume-Kapur artificial earthquake (Newmark et al. 1973) scaled to a peak acceleration of 0.5 g was used in the analyses. This record has a duration of 15 sec and is an average of many typical earthquakes. Viscous damping is introduced by specifying 2% critical damping in the first mode of vibration of the unbraced structure.

Fig. 6 presents the results of a uniform slip-load optimization by FDBFAP for this low-rise structure. The optimum slip load is 134 kN for each device, corresponding to a RPI of 0.219. Fig. 6 also shows that there is very little variation in the relative performance index for local slip loads between 90 kN and 220 kN. This suggests that the seismic response of this structure is not particularly sensitive to variations in the optimum slip load, which may occur due to environmental and construction factors such as temperature change and adjustment variability.

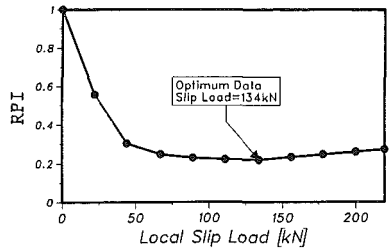

FIG. 6. Slip Load Optimization from FDBFAP: Newmark-Blume-Kapur Artificial Earthquake (0.5 g)

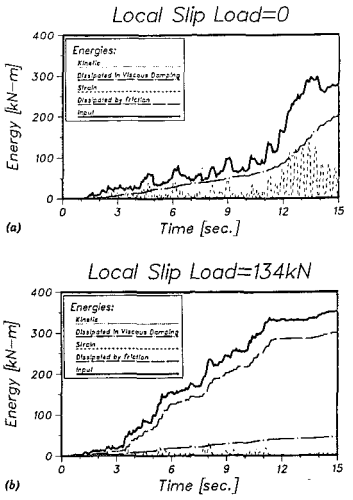

FIG. 7. Energy Time Histories from FDBFAP: Newmark-Blume-Kapur Artificial Earthquake (0.5 g)

The energy time histories as calculated by FDBFAP for the unbraced structure (local slip load = 0) and for the friction-damped frame (local slip load = 134 kN) are presented in Fig. 7. The friction devices are very efficient in reducing the amplitudes of the strain-energy time history and therefore improve the performance of the structure. The maximum strain energy induced in the FDBF is only 23% of the maximum strain energy induced in

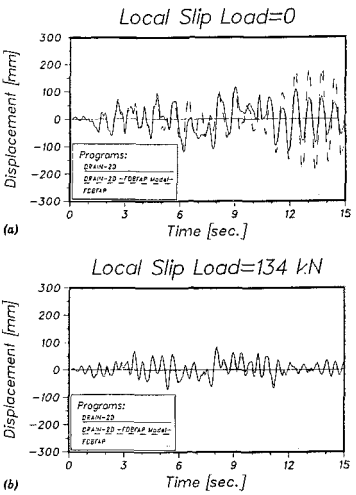

FIG. 8. Top Floor Relative Displacement Time Histories: Newmark-Blume-Kapur Artificial Earthquake (0.5 g)

the unbraced structure. The strain-energy area for the FDBF is only 21% of the strain-energy area for the unbraced frame. At the end of the record, 86% of the input energy has been dissipated by friction.

Fig. 8 presents the top-floor-displacement time histories, relative to the moving base, for the unbraced structure and for the FDBF. The FDBFAP results are identical to the ones obtained with DRAIN-2D incorporating the FDBFAP assumptions. The predictions of DRAIN-2D and FDBFAP for zero local slip load are initially close, but the amplitude agreement becomes poor near the end of the response record. This is due to the severe inelastic deformations predicted by DRAIN-2D for this unbraced case. The members of the FDBF remain elastic at all times and the structural responses predicted by DRAIN-2D and FDBFAP are virtually identical for the entire duration of the earthquake.

Ground-Motion Representation

The steady-state response of a single-story structure equipped with the new friction-damping system and subjected to sinusoidal ground motion has been investigated analytically (Filiatrault and Cherry 1988b). The condition for which the amplitude of the motion is a minimum for a particular ground-excitation frequency ω_g can formally be written

$$\frac{2P_0 \cos \alpha}{ma_g} = F\left(\frac{T_b}{T_u}, \frac{T_h}{T_u}\right) \qquad (3)$$

where P_0 = optimum local slip load of friction damper; α = angle of inclination of diagonal cross-braces with the horizontal; m = total mass of the structure; a_g = peak ground acceleration; T_b = natural period of fully braced structure (no slippage); T_u = natural period of the unbraced structure (all dampers slipping); T_h = period of the harmonic ground motion; F = unknown function.

The significance of Eq. 3 is that it reveals the nondimensional parameters governing the optimum slip load of a one-story FDBF excited by harmonic ground motion. An important conclusion that can be drawn from this result is that the optimum slip load depends on the frequency and amplitude of the ground motion and is not strictly a structural property. Also, it is interesting to note that the value of the optimum slip load is linearly proportional to the peak ground acceleration.

By extension, it may be expected that under seismic loading conditions the optimum slip-load distribution of a friction-damped structure will be influenced by the characteristics of the earthquake ground motion anticipated at the building construction site. Therefore, it becomes necessary to consider a variety of ground motions in any parametric study involving the optimum slip-load distribution.

Since earthquakes are random in nature, it is unlikely that the same earthquake ground motion will be repeated at a given site. The use of specific historical earthquake records may not lead to meaningful results because individual real earthquake records represent a single realization of a set of random parameters (magnitude, focal depth, attenuation characteristics, frequency content, duration, etc.) that will likely never occur again and that may not be satisfactory for design purposes. This shortcoming can be avoided by the use of artificially generated earthquakes of the same class as past observed earthquakes.

A stochastic representation of earthquake ground motion was used in the

parametric study undertaken in this investigation. In this model, proposed by Vanmarcke and Lai (1980) and Lai (1982), the essential transient character of the earthquake ground motion is captured during its strong motion duration, while its equivalent stationary frequency content is represented by the Kanai-Tajimi power spectral density function $S_a(T)$ (Kanai 1957; Tajimi 1960):

$$S_a(T) = \frac{1 + 4h_g^2\left(\frac{T_g}{T}\right)^2}{\left[1 - \left(\frac{T_g}{T}\right)\right]^2 + 4h_g^2\left(\frac{T_g}{T}\right)^2} S_A = |H(T)|^2 S_A \quad \ldots\ldots (4)$$

where $|H(T)|^2$ represents the transfer function of the soil layers and S_A the power spectral density function at the bedrock level. Physically, the Kanai-Tajimi ground power spectral density function is derived from an "ideal white noise" excitation (S_A) at bedrock, which is then filtered appropriately through the overlaying soil deposits.

The computer program created for the simulation of ensembles of artificial-earthquake accelerograms incorporates the power spectral density function defined by Eq. 4 along with a specified value of peak ground acceleration a_g. This acceleration controls the amplitude of the generated accelerogram, and also its duration s_0 in accordance with the findings of Vanmarcke and Lai:

$$s_0 = 30 \exp(-3.254 a_g^{0.35}) \quad \ldots\ldots (5)$$

The Vanmarcke and Lai model offers the advantage of completely describing the ground motion by independent seismic parameters that can be estimated at a given site: the peak ground acceleration a_g, the predominant ground period T_g, and the ground damping h_g.

Due to the fact that most historical earthquake power spectral density functions are quite erratic, it is difficult to determine the parameters of the corresponding smooth Kanai-Tajimi power spectral density function. The "spectral moments" method was proposed by Vanmarcke (1977) to estimate the Kanai-Tajimi parameters from real accelerograms; this method has been used by several investigators (Binder 1978; Lai 1979).

The method of spectral moments has been applied by Vanmarcke and Lai (1980) and Lai (1982) to the data obtained from 140 horizontal acceleration components of 70 western United States strong-motion records. This data set was originally selected by McGuire and Barnhard (1977) so as to be representative of a broad range of earthquake magnitudes, epicentral distances, motion intensities, and site conditions. Based on the method of moving-average statistics, Vanmarcke and Lai have proposed empirical equations for estimating the Kanai-Tajimi parameters (T_g, h_g). These equations involve geophysical information that may be available at a given site. Thus

$$T_g = \frac{2\pi}{27 - 0.09R} \qquad 10 \text{ km} \le R \le 160 \text{ km} \quad \ldots\ldots (6)$$

$$T_g = \frac{2\pi}{65 - 7.5M_L} \qquad 5 \le M_L \le 7 \quad \ldots\ldots (7)$$

$$h_g = 0.32 = \text{constant} \quad \ldots\ldots (8)$$

where R = epicentral distance in km; and M_L = local Richter magnitude.

The joint effects of M_L and R on the Kanai-Tajimi parameters were not considered by Vanmarcke and Lai; therefore discrepancies can result from the use of Eqs. 6 and 7.

Vanmarcke and Lai observed that the Kanai-Tajimi damping (h_g) increases slightly with the local Richter magnitude (M_L) but decided to hold this value constant at 0.32. In the present investigation, a sensitivity analysis using FDBFAP was performed on typical structures in order to study the influence of h_g on the optimum slip-load distribution. The results showed that the optimum slip-load distribution was not influenced significantly by h_g. The ground damping h_g therefore was discarded as a varying parameter and was set to a constant value of 0.32, as proposed by Vanmarcke and Lai.

Parametric Study

Strategy

The effect of various slip-load distributions along the height of friction-damped structures was investigated earlier by Filiatrault and Cherry (1988b). For a general structure subjected to earthquake excitation, numerical analyses support the feasibility of using an optimum slip-shear distribution that is proportional to the interstory displacement (or drift). This displacement is equal to the tangential deviation of adjacent storys and basically results from vibration in the most dominant mode. The slip shear $V_{s(i)}$ at any story i of the structure is related to the total local slip load of that story by

$$V_{s(i)} = \sum_{j=1}^{N_{Di}} 2P_{lij} \cos \alpha_{ij} \quad \ldots\ldots (9)$$

where P_{lij} = local slip load for the jth friction damper in the ith story; α_{ij} = angle of the inclination from the horizontal of the jth braces in the ith story; and N_{Di} = number of friction dampers in the ith story.

However, it has been shown (Filiatrault and Cherry 1988b) that very little benefit is derived from the use of this optimum distribution when compared with the use of the simpler uniform distribution. Therefore, for design purposes, it seems adequate to employ a uniform slip-shear distribution to optimize the seismic response of friction-damped multistory structures. This approach simplifies the design procedure and has the added advantage of eliminating the risk during construction of improperly distributing the friction dampers specified for a structure.

Using such a distribution, an approximate design equation for the total optimum slip shear V_0 can be constructed from the results of a parametric study. The proposed design equation can be written

$$\frac{V_0}{W} = \frac{\sum_{i=1}^{NS} \sum_{j=1}^{N_{Di}} 2P_{0ij} \cos \alpha_{ij}}{W} = M\left(\frac{T_b}{T_u}, \frac{T_g}{T_u}, NS\right) \cdot \frac{a_g}{g} \quad \ldots\ldots (10)$$

where V_0 = total optimum slip shear; W = total weight of the structure; g acceleration of gravity; NS = number of storys and M = an unknown function (or slope).

For fixed values of T_b/T_u, T_g/T_u, and NS, M can be estimated by the least-square method. The sum of the square of the errors I can be written

$$I = \sum_{k=1}^{N_a} \left[\left(\frac{2P_0 \cos \alpha}{W} \right)_k^* - M \cdot \left(\frac{a_g}{g} \right)_k \right]^2 \quad \ldots\ldots (11)$$

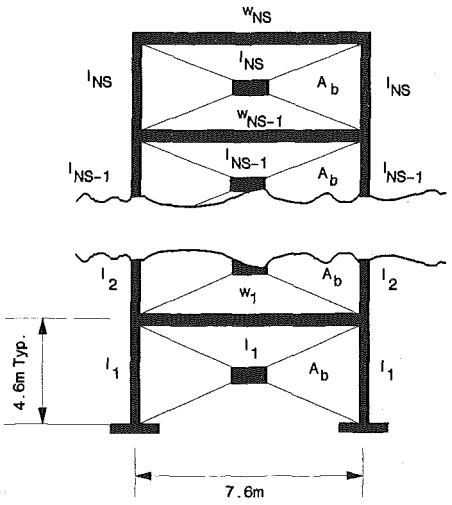

FIG. 9. Basic Structural Configuration Used in Parametric Study

where $(2P_0 \cos \alpha/W)_k^*$ = true optimum slip load obtained with FDBFAP for kth analysis; and N_a = number of analyses with different a_g/g values.

The least-square method consists in minimizing the square of the errors:

$$\frac{\partial I}{\partial M} = 0 \quad \ldots\ldots (12)$$

which leads to a relation for M obtained for particular values of T_b/T_u, T_g/T_u, and NS.

$$M = \frac{\sum_{k=1}^{N_a} \left[\left(\frac{2P_0 \cos \alpha}{W} \right)_k^* \cdot \left(\frac{a_g}{g} \right)_k \right]}{\sum_{k=1}^{N_a} \left[\left(\frac{a_g}{g} \right)_k^2 \right]} \quad \ldots\ldots (13)$$

An array of M values can then be generated for different values of T_b/T_u, T_g/T_u, and NS, from which M in Eq. 10 can be estimated.

Structural Model

The basic structural model used in the parametric study of multistory friction-damped structures is shown in Fig. 9; one, three, five, and ten story versions of this basic structure were examined. Each version has a uniform mass distribution and a mass-proportional unbraced lateral-stiffness distribution:

$$I_i = \frac{\sum_{j=i}^{NS} w_j}{W} I_1 \quad \ldots\ldots (14)$$

where I_i = moment of inertia of the ith floor columns and beams; w_j = weight of the jth floor; and W = total weight of the structure. The same

TABLE 1. Versions of Basic Structural Configuration

NS (1)	Version number (2)	W (kN) (3)	I_1 (mm^4) (4)	T_u (sec) (5)	A_b (mm^2) T_b/T_u = 0.20 (6)	T_b/T_u = 0.40 (7)	T_b/T_u = 0.50 (8)	T_b/T_u = 0.60 (9)	T_b/T_u = 0.80 (10)
1	1	445	3×10^9	0.12	80,927	17,777	—	6,007	1,905
1	2	445	338×10^6	0.37	8,855	1,937	—	656	207
1	3	445	48×10^6	1.00	1,251	274	—	93	29
1	4	445	13×10^6	1.95	329	72	—	24	8
3	1	1,110	42×10^9	0.11	370,990	—	41,938	—	6,452
3	2	1,110	2×10^9	0.49	18,550	—	2,097	—	323
3	3	1,110	416×10^6	1.10	3,710	—	419	—	65
3	4	1,110	125×10^6	2.01	1,113	—	126	—	19
5	1	2,000	125×10^9	0.11	967,800	—	96,780	—	16,130
5	2	2,000	6×10^9	0.53	48,390	—	4,839	—	807
5	3	2,000	1×10^9	1.18	9,678	—	968	—	161
5	4	2,000	416×10^6	2.05	3,226	—	323	—	54
10	1	4,225	31×10^9	0.52	180,656	—	22,582	—	3,226
10	2	4,225	9×10^9	0.96	52,992	—	6,624	—	946
10	3	4,225	2×10^9	2.01	12,044	—	1,505	—	215

diagonal braces were used throughout a structure. The properties of the various structures are listed in Table 1; it may be seen that a total of 45 different structures were considered in this parametric study.

Range of Values Considered

The values of the different variables used in the parametric study of multistory friction-damped structures are given in Table 2. For each combination of parametric values, five different sample accelerograms were simulated by the computer program described previously. The total number of FDBFAP analyses performed was 4,880; the calculations were made with an IBM-PC microcomputer and a SUN 3/260 minicomputer. For each case, the optimum value of the slip load was established from analyses in which a P_l/W increment equal to 0.01 was used. The minimum number of increments was 25; each increment corresponds to one time-history dynamic analysis.

Results for Least Square Slopes, M

Typical results of the parametric study are shown in Fig. 10 which presents the values of V_0/W ($V_0 = 2P_0 \cos \alpha$) obtained for fixed values of NS and T_g/T_u and for all the values of T_b/T_u and a_g/g considered in Table 2. The data are presented along with the least-square slopes M obtained from Eq. 13.

Correlation between M and T_b/T_u

Fig. 11 illustrates typical relations obtained between the least-square slopes M and T_b/T_u for different values of T_g/T_u and a fixed value of NS. It can

TABLE 2. Values of Parameters Used in Parametric Study

Parameter (1)	Values (2)
NS	1, 3, 5, 10
T_g/T_u	0.1 sec/T_u; 0.7 sec/T_u; 1.4 sec/T_u; 2.0 sec/T_u
T_b/T_u	0.20, 0.40, 0.60, 0.80 for NS = 1
	0.20, 0.50, 0.80 for NS = 3, 5, 10
a_g/g	0.005, 0.05, 0.10, 0.15, 0.20, 0.30, 0.40 for NS = 1
	0.05, 0.10, 0.20, 0.40 for NS = 3, 5, 10

J. Struct. Eng. 1990.116:1334-1355.

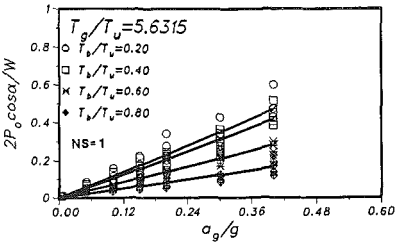

FIG. 10. Typical Results of Parametric Study

be seen that M is negatively correlated with T_b/T_u; the relationship is very nearly linear, such that we can approximate M by:

$$M = a\left(\frac{T_b}{T_u}\right) + b \quad \ldots\ldots (15)$$

where a and b are functions of T_g/T_u and NS.

Fig. 12 presents the estimated values of the parameters a and b along with bilinear least-square fits through the data for different values of NS:

$$a = \begin{cases} (-1.24NS - 0.31)\dfrac{T_g}{T_u} & 0 < \dfrac{T_g}{T_u} \leq 1 \\ \dfrac{(0.01NS + 0.02)T_g}{T_u} - 1.25NS - 0.32 & \dfrac{T_g}{T_u} > 1 \end{cases} \quad \ldots\ldots (16)$$

$$b = \begin{cases} \dfrac{(1.04NS + 0.43)T_g}{T_u} & 0 < \dfrac{T_g}{T_u} \leq 1 \\ \dfrac{(-0.002NS + 0.002)T_g}{T_u} + 1.04NS + 0.42 & \dfrac{T_g}{T_u} > 1 \end{cases} \quad \ldots\ldots (17)$$

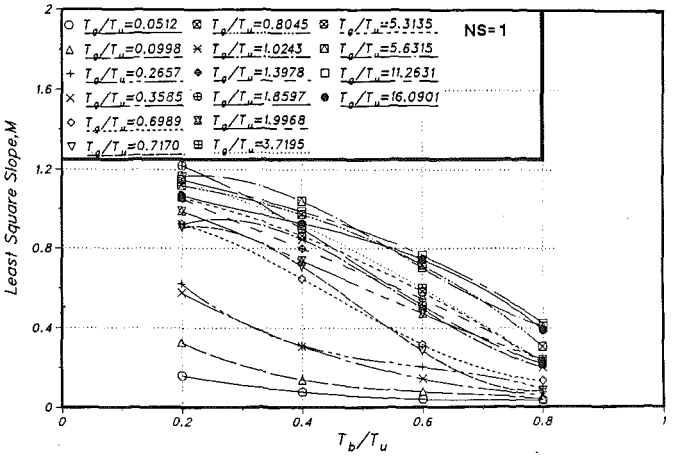

FIG. 11. Correlation Between M and T_b/T_u

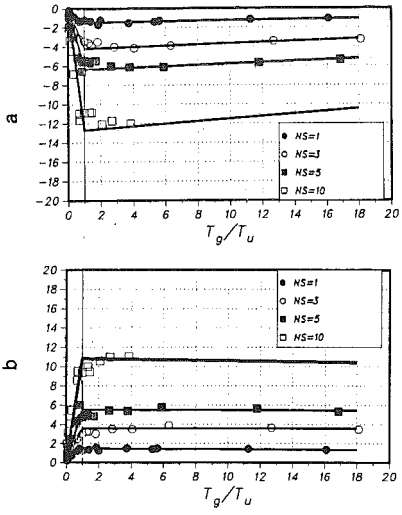

FIG. 12. Least-Square Slope Parameters a and b

Proposed Design Equation

An approximate design equation for the total optimum slip shear V_0 is obtained by substituting Eqs. 15, 16, and 17 into Eq. 10:

$$\frac{V_0}{ma_g} = \begin{cases} \dfrac{\left[\dfrac{(-1.24NS - 0.31)T_b}{T_u} + 1.04NS + 0.43\right]T_g}{T_u} & 0 \leq \dfrac{T_g}{T_u} < 1 \\ \dfrac{\left[\dfrac{(0.01NS + 0.02)T_g}{T_u} - 1.25NS - 0.32\right]T_b}{T_u} & \\ \quad + \dfrac{(0.002 - 0.002NS)T_g}{T_u} + 1.04NS + 0.42 & \dfrac{T_g}{T_u} > 1 \end{cases} \quad \ldots (18)$$

Design Slip Load Spectrum

Eq. 18 can be used directly to estimate the total optimum slip shear V_0. However, a graphical representation of this equation in the form of a design

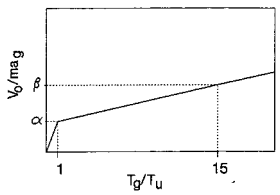

FIG. 13. Construction of Design Slip-Load Spectrum

TABLE 3. Ordinates α and β for Construction of Design Slip-Load Spectrum

	$NS = 1$		$NS = 2$		$NS = 3$		$NS = 4$		$NS = 5$		$NS = 6$		$NS = 7$		$NS = 8$		$NS = 9$		$NS = 10$	
T_b/T_u (1)	α (2)	β (3)	α (4)	β (5)	α (6)	β (7)	α (8)	β (9)	α (10)	β (11)	α (12)	β (13)	α (14)	β (15)	α (16)	β (17)	α (18)	β (19)	α (20)	β (21)
0.20	1.15	1.22	1.94	2.01	2.73	2.80	3.52	3.60	4.31	4.39	5.10	5.18	5.89	5.97	6.68	6.76	7.47	7.55	8.26	8.35
0.25	1.08	1.16	1.80	1.90	2.53	2.64	3.26	3.38	3.99	4.11	4.72	4.85	5.44	5.59	6.17	6.33	6.90	7.07	7.63	7.80
0.30	1.00	1.10	1.67	1.79	2.33	2.47	3.00	3.16	3.66	3.84	4.33	4.52	5.00	5.21	5.66	5.89	6.33	6.58	6.99	7.26
0.35	0.92	1.04	1.53	1.67	2.13	2.31	2.73	2.94	3.34	3.57	3.94	4.20	4.55	4.83	5.15	5.46	5.76	6.09	6.36	6.72
0.40	0.85	0.99	1.39	1.56	1.93	2.14	2.47	2.72	3.01	3.29	3.56	3.87	4.10	4.45	4.64	5.02	5.18	5.60	5.72	6.18
0.45	0.77	0.93	1.25	1.45	1.73	1.97	2.21	2.50	2.69	3.02	3.17	3.54	3.65	4.07	4.13	4.59	4.61	5.11	5.09	5.64
0.50	0.69	0.87	1.11	1.34	1.53	1.81	1.95	2.28	2.36	2.75	2.78	3.22	3.20	3.68	3.62	4.15	4.04	4.62	4.46	5.09
0.55	0.61	0.81	0.97	1.22	1.33	1.64	1.68	2.06	2.04	2.47	2.40	2.89	2.75	3.30	3.11	3.72	3.47	4.14	3.82	4.55
0.60	0.54	0.75	0.83	1.11	1.13	1.47	1.42	1.84	1.71	2.20	2.01	2.56	2.30	2.92	2.60	3.29	2.89	3.65	3.19	4.01
0.65	0.46	0.69	0.69	1.00	0.92	1.31	1.16	1.62	1.39	1.93	1.62	2.23	1.86	2.54	2.09	2.85	2.32	3.16	2.55	3.47
0.70	0.38	0.63	0.55	0.89	0.72	1.14	0.89	1.40	1.07	1.65	1.24	1.91	1.41	2.16	1.58	2.42	1.75	2.67	1.92	2.93
0.75	0.30	0.57	0.41	0.78	0.52	0.98	0.63	1.18	0.74	1.38	0.85	1.58	0.96	1.78	1.07	1.98	1.18	2.18	1.29	2.38
0.80	0.23	0.52	0.27	0.66	0.32	0.81	0.37	0.96	0.42	1.10	0.46	1.25	0.51	1.40	0.56	1.55	0.60	1.69	0.65	1.84

J. Struct. Eng. 1990.116:1334-1355.

slip-load spectrum provides a more convenient and simplified method for establishing V_0. If a plot of V_0/ma_g versus T_g/T_u is made for particular values of T_b/T_u and NS, using Eq. 18, a bilinear curve will be obtained as shown in Fig. 13. This curve represents a general design slip-load spectrum for multistory friction-damped structures. This spectrum is completely described by specifying the ordinate α, representing the upper bound of the first branch of the bilinear curve and corresponding to $T_g/T_u = 1$ for all NS, and any other ordinate data β, compatible with the second linear branch and taken here as the ordinate values at $T_g/T_u = 15$. The ordinates α and β of these points are given by Eq. 18:

$$\alpha = \frac{(-1.24NS - 0.31)T_b}{T_u} + 1.04NS + 0.43 \quad \text{(19)}$$

$$\beta = \frac{(-1.07NS - 0.10)T_b}{T_u} + 1.01NS + 0.45 \quad \text{(20)}$$

The values of α and β have been calculated for different values of T_b/T_u and NS and are presented in Table 3. With the use of this table, a design slip-load spectrum can be quickly constructed for a particular design or retrofit situation.

Choice of Diagonal Cross Braces

In a design situation, different member sizes are available for the diagonal cross braces. Similarly, in the case of seismic retrofit of a structure, it may be decided to replace completely the diagonal cross braces. For a conventional design, the cross braces would be chosen to carry a certain portion of the lateral seismic force. However, in the case of the design or retrofit of a structure equipped with friction devices, the diagonal cross braces should be chosen to optimize the response of the structure. The best choice of cross braces is the one for which the relative performance index (RPI) is the overall minimum among the family of RPI values evaluated at the optimum slip loads corresponding to the available diagonal-member choices. To determine

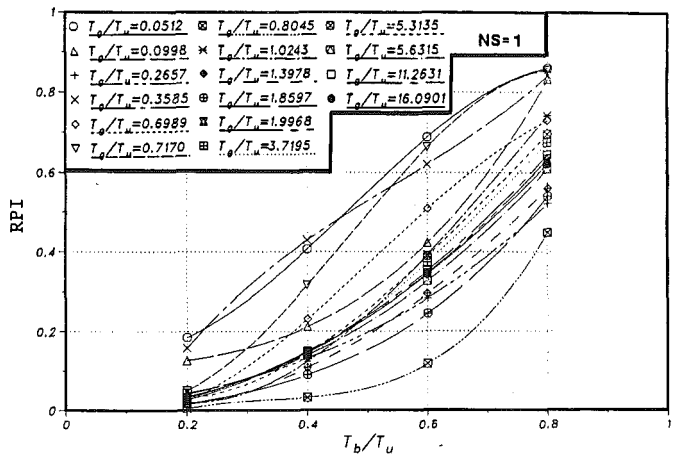

FIG. 14. Average Values of RPI at Optimum Slip Load

that best choice of cross braces, the results of the parametric study can be used to find the value of T_b/T_u that minimizes the RPI when the friction devices are set at their optimum slip loads.

Fig. 14 presents the average values of RPI at the optimum slip load for $NS = 1$ and for different values of T_b/T_u and T_g/T_u. Each point on the curve is an average of 35 RPI values at the optimum slip load taken across the a_g/g values (see Table 1). It can be seen that the RPI is proportional to T_b/T_u and the best response (minimum RPI) is obtained when the values of T_b/T_u are small, which corresponds to large diagonal cross braces. The same trend was observed for other values of NS. Thus, the most suitable diagonal cross braces are those having the largest possible cross-sectional area; this must be balanced against the limitations of cost and the availability of material. Most of the curves in Fig. 14 exhibit steeper slopes for values of T_b/T_u larger than 0.4. Therefore, the diagonal cross braces preferably should be chosen such that $T_b/T_u < 0.40$.

Proposed Design Procedure

Based on the results of the parametric study, the following procedure is proposed for the seismic design of friction-damped structures.

Step 1

In the case of a new structure, design the unbraced moment-resisting frame to carry safely the usual load combinations but without considering earthquake effects.

In the situation of retrofit of an existing building, verify that the unbraced moment-resisting frame can carry safely the usual load combinations but without considering earthquake effects.

It is assumed that the friction dampers will fully dissipate the seismic energy. The designer may choose to include earthquake loads in the load combination in order to fall back on conventional ductility design as an added factor of safety in the event of a catastrophic earthquake.

Step 2

Calculate the fundamental period of the unbraced structure, T_u.

Choose sections for the diagonal cross braces such that $T_b/T_u < 0.40$, if economically possible.

Estimate the peak ground acceleration a_g and the predominant ground period T_g for the construction site. In Canada, a_g can be taken directly from the *National Building Code of Canada* (1985); the values in that reference are based on a probability of exceedence of 10% in 50 years. However, at present, no maps exist in Canada for determining T_g. If historic accelerogram records or soil-boring logs that allow T_g estimates to be made for the construction site are not available, it is recommended that T_g be aproximated by the empirical formulas proposed by Vanmarcke and Lai (Eqs. 6 and 7).

Step 3

Verify that the nondimensional ratios fall within the following limits:

$$0.20 \le \frac{T_b}{T_u} \le 0.80 \qquad 0.05 \le \frac{T_g}{T_u} \le 20 \qquad 0.005 \le \frac{a_g}{g} \le 0.40 \qquad NS \le 10$$

These bounds correspond to those used in the present study and represent reasonable practical limits. If the inequalities are not verified, the optimum slip load should be determined from dynamic analyses (FDFAP).

Step 4

Determine the coefficients α and β from Table 3 and construct the appropriate design slip-load spectrum as indicated in Fig. 13.

Step 5

Use the constructed design slip-load spectrum to estimate the total slip shear V_0. Distribute this total slip shear uniformly among the floors of the structure.

$$V_{s(i)} = \frac{V_0}{NS} \quad \ldots\ldots (21)$$

where $V_{s(i)}$ = slip shear in the ith floor.

Step 6

Distribute the slip shear of each floor $V_{s(i)}$ among the number of friction dampers inserted in each floor.

$$\sum_{j=1}^{N_{Di}} 2P_{0ij} \cos \alpha_{ij} = V_{s(i)} \quad \ldots\ldots (22)$$

where N_{Di} = number of friction dampers inserted in the ith floor.

Step 7

Calculate the axial loads induced in the cross braces from wind effect and verify that the friction dampers are not slipping under these loads (see Eq. 1) using the following expressions. For slender braces ($P_{0ij} > P_{(cr)ij}$):

$$P_{0ij} \geq \frac{P_{wij} + P_{(cr)ij}}{2} \quad \ldots\ldots (23)$$

For stubby braces ($P_{0ij} \leq P_{(cr)1ij}$):

$$P_{0ij} \geq P_{wij} \quad \ldots\ldots (24)$$

where P_{wij} = axial wind load induced in the tensile diagonal brace of the jth braced bay of the ith floor; and $P_{(cr)ij}$ = corresponding buckling load of that brace.

If Eqs. 23 or 24 are not verified, choose one of the following two alternatives: (1) Use the value of the slip load satisfying the equality in Eqs. 23 or 24 and perform dynamic analyses (FDBFAP) to examine the response of the structure; or (2) modify the unbraced moment-resisting frame to carry a larger portion of the wind load and return to Step 2.

Step 8

Estimate the tensile-yield load of the cross braces and verify that these cross braces do not yield before slipping occurs using the following expressions. For slender braces ($P_{0ij} > P_{(cr)ij}$):

$$P_{0ij} \leq \frac{A_{bij}\sigma_{yij} + P_{(cr)ij}}{2} \quad \ldots\ldots (25)$$

For stubby braces ($P_{0ij} \leq P_{(cr)ij}$):

$$P_{0ij} \leq A_{bij}\sigma_{yij} \quad \ldots\ldots (26)$$

where A_{bij} and σ_{yij} = cross-sectional area and tensile-yield stress for the jth tensile brace in the ith floor.

If Eqs. 25 or 26 are not verified, choose one of the following two alternatives: (1) Use a value of the slip load satisfying the equality in Eqs. 25 or 26 and perform dynamic analyses (FDBFAP) to examine the response of the structure; or (2) increase the size of the diagonal cross braces and return to Step 3.

DESIGN EXAMPLE

To illustrate the use of the proposed design procedure assume that the low-rise frame shown in Fig. 5 is to be retrofitted with friction dampers.

Step 1

This structure was designed originally by Montgomery and Hall (1979). Assume that the unbraced structure can carry safely the usual load combinations without considering earthquake effect.

Step 2

The fundamental periods of the structure were calculated to be $T_u = 0.72$ sec; and $T_b = 0.38$ sec.

Let the Eureka, California, earthquake, December 21, 1954, COMP N46W, be the design earthquake specified for the construction site (Vancouver, Canada). The parameters for this seismic event were determined by Vanmarcke and Lai (1980): $a_g = 0.20$ g [which is equal to the NBCC (*National* 1985) value assigned to Vancouver]; and $T_g = 0.69$ sec.

Step 3

Verify that the nondimensional ratios are within the appropriate limits:

$$0.20 \leq \frac{T_b}{T_u} = 0.53 \leq 0.80 \qquad 0.50 \leq \frac{T_g}{T_u} = 0.96 \leq 20$$

$$0.005 \leq \frac{a_g}{g} = 0.20 \leq 0.40 \qquad NS = 3 \leq 10 \quad \ldots\ldots\ldots\ldots\ldots\ldots\ldots\ldots \quad (27)$$

Step 4

The coefficients α and β are estimated from Table 3: $\alpha = 1.43$; and $\beta = 1.73$.

Step 5

The design slip-load spectrum is constructed as shown in Fig. 15. From this spectrum the total optimum slip shear is estimated as

$$\frac{V_0}{ma_g} = 1.14 \quad \text{or} \quad V_0 = 514.44 \text{ kN} \ldots\ldots\ldots\ldots\ldots\ldots\ldots\ldots\ldots\ldots \quad (28)$$

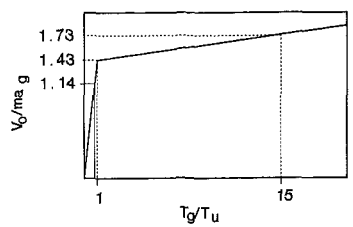

FIG. 15. Design Slip-Load Spectrum for Design Example

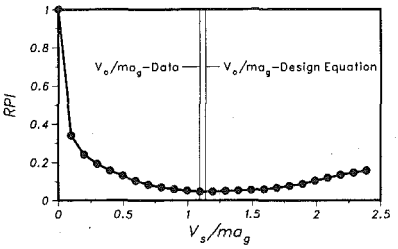

FIG. 16. Optimum Slip-Load Study for Design Example

This slip shear is distributed uniformly among the floors:

$$V_{s(i)} = 171.48 \text{ kN}; \qquad i = 1, 2, 3 \quad \ldots\ldots (29)$$

Step 6

The optimum local slip load P_0 for each friction damper is

$$P_0 = \frac{V_{s(i)}}{2 \cos \alpha} = 90.75 \text{ kN} \quad \ldots\ldots (30)$$

Step 7

It is assumed that this structure is located in Vancouver. The design wind pressure acting on the building is calculated by the *National Building Code of Canada* (1985).

A static analysis of the structure reveals that the maximum axial load induced by the wind in the diagonal cross braces is 11.48 kN. The buckling load for a cross-brace member (2L75 × 75 × 6) is estimated to be 97.10 kN: the braces will not buckle under the design wind load.

From Eq. 26:

$$P_{0ij} = 90.75 \text{ kN} \qquad i = 1, 2, 3; \quad j = 1$$

$$P_{wij} = 11.48 \text{ kN} \qquad i = 1, 2, 3; \quad j = 1 \qquad \therefore P_{0ij} \geq P_{wij} \quad \ldots\ldots (31)$$

The friction dampers will not slip under the design wind load.

Step 8

Assuming a tensile-yield stress σ_{yij} equal to 300 MPa for the diagonal cross braces, verify Eq. 26:

$$P_{0ij} = 90.75 \text{ kN} \qquad i = 1, 2, 3; \quad j = 1$$

$$A_{bij}\sigma_{yij} = 327.25 \text{ kN} \qquad i = 1, 2, 3; \quad j = 1 \qquad \therefore P_{0ij} \leq A_{bij}\sigma_{yij} \quad \ldots\ldots (32)$$

Hence the friction dampers will slip before yielding of the cross braces occurs. In fact, the cross-sectional area of the braces is significantly larger than the area necessary to carry the optimum slip load. Reducing the area of the braces would reduce the stiffness of the braced frame and consequently alter the optimum slip load. The designer could iterate to reduce the difference between the diagonal yield and slip load. However, since this example is concerned with the retrofit problem, the brace area of the original structural design has been used.

The optimum slip load obtained from the design slip load spectrum is compared in Fig. 16 with the value obtained from FDBFAP. The two results agree very closely.

Conclusion

The investigation described in this paper represents the first known attempt to develop a simplified method for the seismic design of friction-damped structures.

A specialized computer program was used to obtain the optimum slip-load distribution for the friction devices by minimizing a relative performance index (RPI) derived from energy concepts.

The results of a parametric study on multistory friction-damped braced frames were used to construct a general design slip-load spectrum for a quick evaluation of the total optimum slip shear in a multistory building. The spectrum takes into account the properties of the structure and of the ground motion anticipated at the construction site. The availability of this design slip-load spectrum should lead to a greater acceptance by the engineering profession of this innovative design concept.

Appendix I. References

Binder, R. (1978). "Seismic safety analysis of multi-degree-of-freedom inelastic structures," thesis presented to the Massachusetts Institute of Technology, at Cambridge, Mass., in partial fulfillment of the requirements for the degree of Master of Science.

Filiatrault, A., and Cherry, S. (1987). "Performance evaluation of friction damped braced steel frames under simulated earthquake loads." *Earthquake Spectra*, 3(1), 57–78.

Filiatrault, A., and Cherry, S. (1988a). "Comparative performance of friction damped systems and base isolation systems for earthquake retrofit and aseismic design." *Earthquake Engrg. and Struct. Dynamics*, 16(3), 389–416.

Filiatrault, A., and Cherry, S. (1988b). "Seismic design of friction damped braced steel plane frames by energy methods." *Earthquake Engrg. Res. Lab. Report, UBC-EERL-88-01*, Dept. of Civ. Engrg., Univ. of British Columbia, Vancouver, Canada.

Filiatrault, A., and Cherry, S. (1989). "Efficient numerical modelling for seismic design of friction damped braced steel plane frames." *Canadian J. of Civ. Engrg.*, 16(3), 211–218.

Kanai, K. (1957). "Semi-empirical formula for the seismic characteristics of the ground." *Bulletin of the Earthquake Res. Inst.*, Univ. of Tokyo, Tokyo, Japan, 35(16), 309–325.

Kannan, A. E., and Powell, G. M. (1973). "DRAIN-2D a general purpose computer program for dynamic analysis of inelastic plane structures." *EERC73-6*, Earthquake Engrg. Res. Ctr., Univ. of California, Berkeley, Calif.

Lai, S. P. (1979). "Ground motion parameters for seismic safety assessment." *Seismic safety of buildings: International study report no. 17*, Massachusetts Inst. of Tech., Cambridge, Mass.

Lai, S. P. (1982). "Statistical characterization of strong ground motions using power spectral density functions." *Bulletin of the Seismological Soc. of Amer.*, 72(1), 259–274.

McGuire, R. K., and Barnhard, J. A. (1977). "Magnitude, distance and intensity data for C.I.T. strong motion records." *U.S. Geological Survey Res. J.*, 5(4), 437–443.

Montgomery, C. J., and Hall, W. J. (1979). "Seismic design of low-rise steel buildings." *J. Struct. Div.*, ASCE, 105(10), 1917–1933.

National building code of Canada, 1985. (1985). NRC No. 23174F, National Research Council of Canada, Ottawa, Ontario, Canada.

Newmark, N. M., Blume, J. A., and Kapur, R. R. (1973). "Seismic design spectra for nuclear power plants." *J. Power Div.*, ASCE, 99(2), 287–303.

Pall, A. S., and Marsh, C. (1982). "Response of friction damped braced frames." *J. Struct. Div.*, 108(6), 1313–1323.

Pall, A. S., Verganalakis, V., and Marsh, C. (1987). "Friction dampers for seismic

control of Concordia University Library building." *Proc., 5th Canadian Conf. on Earthquake Engrg.*, Ottawa, Canada, 191–200.
Tajimi, H. (1960). "A statistical method of determining the maximum response of building structures during an earthquake." *Proc., 2nd World Conf. on Earthquake Engrg.*, Tokyo and Kyoto, Vol. 2, 781–797.
Vanmarcke, E. H. (1977). "Structural response to earthquakes." *Seismic risk and engineering decisions*, C. Lomnitz and E. Rosenblueth, eds., Elsevier Publishing Co., New York, N.Y.
Vanmarcke, E. H., and Lai, S. P. (1980). "Strong motion duration and RMS amplitude of earthquake records." *Bulletin of the Seismological Soc. of Amer.*, 70(4), 1293–1302.

APPENDIX II. NOTATION

The following symbols are used in this paper:

a, b = least-square slope parameters;
a_g = peak ground acceleration;
F = unknown function;
g = acceleration of gravity;
$|H(T)|$ = soil transfer function;
h_g = ground damping;
I = moment of inertia;
m = total mass of structure;
M = least-square slope;
M_L = local Richter magnitude;
NS = number of storys;
P_{cr} = critical Euler buckling load;
P_l = local slip load;
P_w = axial wind load;
P_0 = optimum local slip load;
P_1, P_2 = axial loads;
P_g = global slip load;
R = epicentral distance;
RPI = relative performance index;
S_A = power spectral density function of ground acceleration at bedrock level;
$S_a(T)$ = power spectral density function of ground-surface acceleration;
SEA = strain-energy area for friction-damped structure;
$SEA_{(0)}$ = strain-energy area for unbraced structure (slip load = 0);
s_0 = strong motion duration of earthquake accelerogram;
T = period;
T_b = natural period of braced structure;
T_g = predominant ground period;
T_h = period of harmonic ground motion;
T_u = natural period of unbraced structure;
t = time;
U_{max} = maximum strain energy for friction-damped structure;
$U_{max(0)}$ = maximum strain energy for unbraced structure (slip load = 0);
V = lateral seismic load;
V_s = slip shear;
V_0 = total optimum slip shear;
W = total weight of structure;
α, β = ordinates to construct design slip load spectrum;
$\cos \alpha$ = angle of inclination of diagonal braces from horizontal; and
ω_g = ground excitation frequency.